Simulation of Uniformly Distributed Vibration Effects on a Reciprocal Fiber-optic Polarimetric Current Sensors

P. Tantaswadi and C. Tangtrongbenchasil
Sirindhorn International Institute of Technology, Electrical Engineering Program, Thammasat University
PO Box 22, Thammasat Rangsit, Post Office, Pathumthani 12121

Abstract

Mechanical vibration affects the accuracy of optical fiber current sensor causing error in optical current measurement. In practice, the sensing part of the optical sensor is susceptible to environmental perturbations such as mechanical vibration to the sensing fiber. Reciprocal polari-metric sensor configuration can reduce current measurement error due to the vibration. The accuracy of our model is within 0.01% of the actual value and satisfies application in metering.

Keywords – fiber optic current sensor, uniformly distributed vibration effect, polarimetric current sensor.

1. INTRODUCTION

Fiber optic current sensors rely on Ampere's law and Faraday effects. These are used in the electric power industry for revenue metering, relay, protec-tion and control. The advantages over conven-tional current transformers (CTs) include broad linear dynamic range (more than five orders of magnitude), broad bandwidth (DC to many MHz), no hysteresis, and by proper design, insensitivity to electro-magnetic interference (EMI) and radio-frequency interference (RFI).

Several approaches of fiber optic current sensor based on Faraday effect has been demonstrated [1]. Fiber-optic current sensors have several advantages over conventional CTs, but they have yet to overcome undesirable susceptibility to environ-mental perturbations, *e.g.* temperature, and acoustic vibrations in the sensing part [1]–[2]. One ap-proach is unidirectional polarimetric technique but it suffers from both linear and circular birefrin-gences in the sensing fiber. A reciprocal polarimetric current sensor configuration has been presented to counter the birefringences error. The vibrations affect the birefringence property of the fiber in the sensing part. Unidirectional polari-metric current sensors suffer from environmental perturbations due to varying birefringence in the sensing part [2]. The results are shown in false current readings from environmental perturbations.

In this paper, we show a reciprocal fiber optic current sensor configuration including normalized contrast ratio, and effects of uniformly distributed vibration on the sensor. The accuracy of this sensor is within 0.01% of the actual value and satisfies application in metering (accuracy of 0.3%).

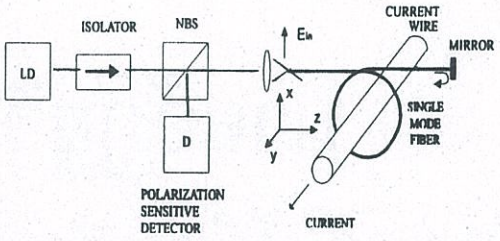

Figure 1 Reciprocal fiber optic polarimetric current sensor configuration, LD: laser diodes, NBS: non-polarizing beam splitter

2. SENSOR PRINCIPLES

Based on magneto-optic Faraday effect, when light propagates in an optical fiber wound around a current carrying wire (see Figure 1), the induced magnetic field causes a rotation of the linear polarization plane of light wave. This angle of Faraday rotation, ΔF, through which the plane of polarization rotates, is given by

$$\Delta F = V \oint_C \vec{H} \cdot d\vec{l} \,, \qquad (1)$$

where V is the Verdet constant of the optical fiber, $\vec{H}$ is the magnetic field intensity along the direction of light propagation, and l is the optical path along the fiber loop. Relying on Ampere's law, this closed loop integral of magnetic field around a wire is proportional the current, I, flowing through it, *i.e.*

$$I = \oint_C \vec{H} \cdot d\vec{l} \,. \qquad (2)$$

Therefore, the angle of rotation, ΔF in the fiber loop configuration is given by

$$\Delta F = VNI, \tag{3}$$

where N is the number of turns of optical fiber wrapped around the current carrying wire. The stability of Faraday rotation based current sensors, through the Verdet constant, depends on source wavelength and temperature.

To measure current I, with constants N and V, we can use a polarimetric sensor to measure ΔF. For the conventional unidirectional polarimetric current sensors, linearly polarized light is launched into a single-mode sensing fiber and a Wollaston prism for evaluation of the current and static linear birefringence [3]-[4] analyzes the output polarization. In practice, light travels through the fiber loop exhibiting additional linear birefringence due to bending and twist-induced circular birefringence can be described by Jones calculus (see next section). These birefringences affect the accuracy and sensitivity to environmental perturbations *i.e.* vibrations of the sensor. Reciprocal fiber-optic current sensors (see Figure 1) interrogate the light in both directions. Since linear and twist-induced birefringences exhibit reciprocal characteristics, the reciprocal rotation of these birefringences cancel when light propagates along and is back-reflected down a fiber. The Faraday magneto-optic effect exhibits nonreciprocal characteristics but the Faraday rotation doubles when light propagates along and is back-reflected down a fiber. Thus, this optical configuration has the advantage to minimize the birefringence induced offset problems associated with the unidirectional polarimetric current sensor.

3. MATHEMATICAL DESCRIPTIONS OF A RECIPROCAL FIBER-OPTIC POLARIMETRIC CURRENT SENSOR

We assume that vibration on the sensing part of optical fiber is uniformly distributed. Then, we analyze for uniformly distributed vibration on reciprocal fiber-optic polarimetric current sensor.

Firstly we launched input light to non-polarizing beam splitter and passes though single-mode fiber with input angle (η) of 45°. Then it continues to forward path of fiber loop to mirror. After that it travels back to the backward path of fiber loop and go to the same path. The following composite Jones Matrix [5]-[6] describing the system is given by

$$E_{out} = \begin{bmatrix} E_x \\ E_y \end{bmatrix} = \frac{1}{2}\bar{L}\cdot M\cdot \bar{L}\cdot R(\eta)\cdot E_{in}, \tag{4}$$

$$E_{in} = \begin{bmatrix} E_x = 1 \\ E_y = 0 \end{bmatrix} = \begin{bmatrix} 1 \\ 0 \end{bmatrix}, \tag{5}$$

$$R(\eta) = \begin{bmatrix} \sin\eta & \cos\eta \\ -\cos\eta & \sin\eta \end{bmatrix}, \tag{6}$$

$$\bar{L} = \begin{bmatrix} A & -B \\ B & A^* \end{bmatrix}, \tag{7}$$

$$\bar{L} = \begin{bmatrix} C & -D \\ D & C^* \end{bmatrix}, \tag{8}$$

$$A = \cos\frac{\alpha}{2} + j\sin\frac{\alpha}{2}\cos(\chi), \tag{9}$$

$$B = \sin\frac{\alpha}{2}\sin(\chi), \tag{10}$$

$$C = \cos\frac{\beta}{2} + j\sin\frac{\beta}{2}\cos(\zeta), \tag{11}$$

$$D = \sin\frac{\beta}{2}\sin(\zeta), \tag{12}$$

$$\alpha = \sqrt{4(VNI+T)^2+\delta^2}, \tag{13}$$

$$\beta = \sqrt{4(VNI-T)^2+\delta^2}, \tag{14}$$

$$\tan\chi = \frac{2(VNI+T)}{\delta}, \tag{15}$$

$$\tan\zeta = \frac{2(VNI-T)}{\delta}. \tag{16}$$

4. ANALYSIS OF THE NORMALIZED CONTRAST RATIO (K)

The Wollaston prism is aligned at 45° and -45° to the birefringence axis of the output end of the sensing fiber. The contrast ratio (K) is defined as

$$K = \frac{I_{45^\circ} - I_{-45^\circ}}{I_{45^\circ} + I_{-45^\circ}} \tag{17}$$

Then, we can derive Eq (4) by using Eq (5) to (12) as:

$$K = -\cos(\alpha)\cos(\beta) + \cos(\zeta-\chi)\sin(\alpha)\sin(\beta) \tag{18}$$

For ideal case, T and $\delta \approx 0$ are negligible, so Eq (18) becomes

$$K_{ideal} = -\cos(4VNI) \tag{19}$$

However, in practice, the use of high circular birefringence T or "spun" fiber ($VNI, \delta << T$, e.g. $\delta = 1.9\pi, T = 120\pi$) can overcome the intrinsic linear birefringence. This K is called K_{dc}, which is (see Appendix)

$$K_{dc} = -\cos(4VNI) + \frac{\delta^2}{\alpha\beta}\sin(\alpha)\sin(\beta) \tag{20}$$

To understand the performance of this sensor, we show the characteristic plot of the deviation of K (ΔK), which is

$$\Delta K(\%) = \frac{K - K_{dc}}{K_{dc}} \times 100\% \qquad (21)$$

In this sensor, Figure 2 shows that the deviation of K in percentage is within 0.01 % of ideal case (T, $\delta \approx 0$) when the range of the linear and circular birefringences are (1.8π, 2.0π) and (119.5π, 120.5π) radians, respectively.

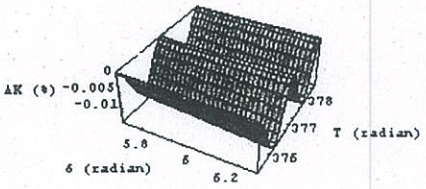

Figure 2 The deviation of K (ΔK) when VNI = 0.01 π radians as a function of δ is between 1.8 π and 2.0 π radians T is between 119.5 π and120.5 π radians.

5. DEVIATION OF K (ΔK) Vs LINEAR BIREFRINGENCE

This sensor exhibits small dependence on linear birefringence. Figure 3 shows that the absolute value of the deviation of K in percentage is below 1×10^{-4}% when δ is between -2 π and 2 π radians when VNI = 0.01 π and T = 120 π radians. Using Eq (18), (20), and (21), $\Delta K(\%)$ is given by

$$\Delta K(\%) = 2.59616\times10^{-6}\delta^2 - 9.24994\times10^{-5}. \qquad (22)$$

In Figure 3 gives maximum δ to achieve the accuracy of 9.24994×10^{-5}% for revenue metering application from Eq (22) is 0 *rad.*

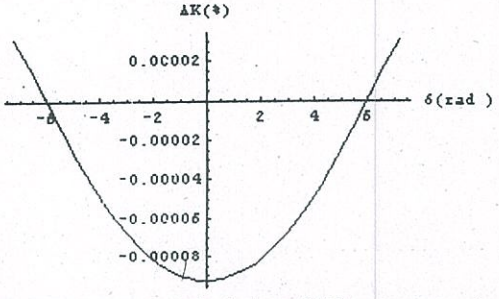

Figure3 Simulated deviation of K in percent varies with linear birefringence (VNI = 0.01π, T = 120π).

6. APPENRENT CURRENT VS LINEAR BIREFRINGENCE

Acoustic vibration on the sensing fiber can cause angular rotation of light wave polarization and may affect birefringence property of the sensing fiber [8]. The result could be misread as an actual current. Mechanical vibrations with a magnitude of 3.0 $g_{p\text{-}p}$ (1g = 9.8m/s^2) applied to a sensing fiber of unidirectional polarimetric sensor can cause an apparent current of 400 $A_{p\text{-}p}$. Simulated apparent current (T = 120 π, δ_v = 0.3 sin (2π f_v t), and the total linear birefringence is assumed to vary between 1.8π and 2.0π radians) for this sensor is shown in Figure 4. The frequency of vibration or varying linear birefringence (f_v) is chosen to be 50 Hz, which is common to electric power systems [1]. Very small apparent currents of less than $2.5\text{x}10^{-8}$ Amperes for 633 nm wavelength when the total linear birefringence δ is (1.8π, 2.0π) radians and theδ_v is shown in Figure 4(a).

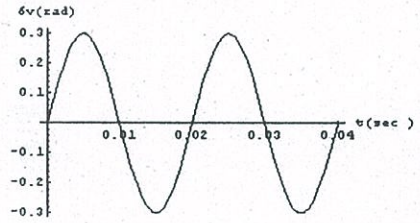

(a)

(b)

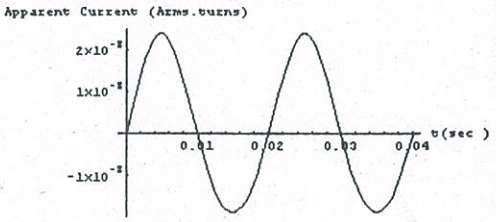

Figure4 Simulated apparent current (b) in Amperes. turns Vs birefringence (a) (VNI= 0 and T= 120π)

7. DISCUSSION AND CONCLUSION

The mathematical modeling of reciprocal fiber-optic current sensor configuration is demonstrated. The performance of the current sensor is similar to that of the ideal case (δ, $T \approx 0$). To satisfy the conditions of $\frac{\delta}{2T} \ll 1$ and $VNI \cdot \delta \cdot T$ helical winding on an acrylic torus is presented. We can find the normalized contrast

ratio K being affected by undesired changes in linear birefringence δ caused by acoustic vibrations and circular birefringence T. For large T, deviation of K (%) is a quadratic function of δ but the contribution of vibrations is small and within 0.01 % (0.01 % of the actual value required for applications in metering). The apparent current shows that the susceptibility of sensor to varying linear birefringence is small and negligible.

8. REFERENCES

[1] S. Short, et al. Elimination of Bbirefringence Induced Scale Factor Errors in the in-line Sagnac Interferometer Current Sensor. *IEEE J-LT*, **16**(10): 1844-1850, October 1998.

[2] S. Short, P. Tantaswadi, et al. Environmental Sensitivity Comparison of in-line Sagnac and Polarimetric Type Current Sensor. *IEEE Trans. Power Delivery*, **11**(4): 1702-1706, 1996.

[3] Z. Ren, et al. Discrimination Between Linear Birefringence and Faraday Rotation in Optical Fiber Current Sensors by Polarization Multiplexing. *Fiber Optic and Laser Sensors VII*, **1169**: 226-232, 1989.

[4] P. Menke and T. Bosselmann. Temperature Compensation in magnetooptic AC Current Sensors using an Intelligent AC-DC Signal Evaluation. *IEEE J-LT*, **13**(7): 1362-70, (1995).

[5] Tabor, et. al Electromagnetic Propagation Through Materials Possesing Both Faraday Rotation and Birefringence: Experiments with Ytterrbium Orthoferrite. *J. Appl. Phys.*, **40**(7): 2760.

[6] A. Smith. Polarization and Magnetooptic Properties of Single-mode Optical Fibre. *Appl. Opt.*: **17**(52), (1978).

[7] S. Short, P. Tantaswadi, et al. (1996) Environmental Sensitivity Comparison of in-line Sagnac and Polarimetric Type Current Sensor. *IEEE Trans. Power Delivery*, **11**(4): 1702-1706 (1996).

[8] K. Grattan and B. Meggit, ed. Optical Fiber Current Measurement. *Optical Fibers Sensor Technology*, **Vol. 1**, Chapman & Hall: 432-438, (1995).

9. ACKNOWLEDGEMENTS

Funding was provided by Thai Research Foundation (TRF) and partially by Thaikhadi Research Institute, Thammasat University. The authors would like to thank Dr. James N. Blake of Nxtphase, USA, Prof. Alan J. Rogers of University of Surrey, UK, and Assoc. Prof. Dr. Pichet Limsuwan of King Mongkut's University of Technology, Thonburi for help and fruitful discussions.

10. APPENDIX

To verify K_{dc}, From Eq (18)

$K = -\cos(\alpha)\cos(\beta) + \cos(\zeta - \chi)\sin(\alpha)\sin(\beta)$

K_{dc} is occurred in practical when $\delta = 1.9\pi$ and $T = 120\pi$, $T \gg VNI$ and

$$\left(\frac{\delta}{2(T+VNI)}\right)^2 \approx \left(\frac{\delta}{2(T-VNI)}\right)^2 \ll 1.$$

$$\text{So } \alpha \approx 2(T+VNI)\sqrt{1+\left(\frac{\delta}{2\cdot(T+VNI)}\right)^2}$$

$$\approx 2(T+VNI)\left(1+\frac{1}{2}\left(\frac{\delta}{2(T+VNI)}\right)^2\right)$$

$$\approx 2(T+VNI)$$

where $\sqrt{1+x} \approx 1+\frac{x}{2}, \quad x \ll 1,$

$$\beta \approx 2(T-VNI)\sqrt{1+\left(\frac{\delta}{2\cdot(T-VNI)}\right)^2}$$

$$\approx 2(T-VNI)\left(1+\frac{1}{2}\left(\frac{\delta}{2(T-VNI)}\right)^2\right),$$

$$\approx 2(T-VNI)$$

where $\sqrt{1-x} \approx 1-\frac{x}{2}, \quad x \ll 1$

then, $\alpha - \beta = 4VNI$, the first term on the right-hand side of Eq (18) becomes

$$-\cos(\alpha)\cos(\beta) = -\cos(\alpha-\beta)$$
$$= -\cos(4VNI)$$

and $\cos(\zeta-\chi) = \cos(\zeta)\cos(\chi) + \sin(\zeta)\sin(\chi)$, using Eq (15) and (16) to obtain

$$\cos(\zeta-\chi) = \frac{\delta^2}{\alpha\beta} + \frac{4}{\alpha\beta}(T^2 - VNI^2)$$

when VNI is very small and $2T \approx \alpha \approx \beta$, then $\cos(\zeta-\chi)$ become

$$\cos(\zeta-\chi) = \frac{\delta^2}{\alpha\beta} - 1$$

Substitute into Eq (18), to get

$$K_{dc} = -\cos(\alpha)\cos(\beta) - \sin(\alpha)\sin(\beta) + \frac{\delta^2}{\alpha\beta}\sin(\alpha)\sin(\beta)$$

$$= -\cos(\alpha-\beta) + \frac{\delta^2}{\alpha\beta}\sin(\alpha)\sin(\beta)$$

$$= -\cos(4VNI) + \frac{\delta^2}{\alpha\beta}\sin(\alpha)\sin(\beta)$$